Fırat Üniversitesi Müh. Bil. Dergisi
37(2), 685-698, 2025

Araştırma Makalesi
https://doi.org/10.35234/fumbd.1665680

Investigation of the Bioactivity Properties of $TiZrCrNb_{0.3}Ta_{0.07}$ Medium Entropy Alloy Produced from TNTZ Waste

Nihal YAYLA[1*], Ömer GÜLER[2], Yakup SAY[3], Harun GÜZEL[4]

[1] Department of Strategic Raw Materials and Advanced Technology Applications, Munzur University, Tunceli, Türkiye
[2] Rare Earth Elements Application and Research Center, Munzur University, Tunceli, Türkiye
[3] Department of Metallurgical and Materials Engineering, Munzur University, Tunceli, Türkiye
[4] Department of Metallurgical and Materials Engineering, Mersin University, Mersin, Türkiye
[*1] nhlyayla@gmail.com, [2] omerguler@munzur.edu.tr, [3] yakupsay@munzur.edu.tr, [4] harun.guzel@etikrom.com

Geliş/Received: 27/03/2025 **Kabul/Accepted: 14/05/2025**

Abstract: High entropy alloys (HEAs) and medium entropy alloys (MEAs) have garnered significant attention as alternative materials in various fields due to their superior physical and chemical properties compared to conventional alloys. One of the most promising applications of this innovative material class is in biomaterials. In this study, a bio-medium entropy alloy (BioMEA), $TiZrCrNb_{0.25}Ta_{0.05}$, was successfully synthesized using non-toxic elements (Ti, Zr, Cr, Nb and Ta) through arc melting of TNTZ alloy waste. The produced BioMEA was comprehensively characterized using scanning electron microscopy (SEM), energy dispersive spectroscopy (EDS), and X-ray diffraction (XRD) to analyze its structural and chemical properties. Additionally, the in-vitro degradation, ion release, and bioactivity properties of the alloy were evaluated and compared with those of the conventional TNTZ alloy, with a focus on the effects of heat treatment. The results demonstrated that heat treatment did not cause significant changes in the microstructure of the $TiZrCrNb_{0.25}Ta_{0.05}$ alloy but led to the formation of intermetallic compounds such as Cr_2Zr and Cr_2Ta on the surface. Degradation tests revealed an unexpected mass gain across all sample groups after a four-week immersion period due to surface precipitation, surpassing the expected mass loss from degradation. Ion release analyses showed similar behavior between the $TiZrCrNb_{0.25}Ta_{0.05}$ and TNTZ alloys, with ion release levels in the ppb range, confirming that Ti was released at non-toxic levels. Bioactivity tests identified low lesvels of Ca-P-O deposition on all sample surfaces, with the highest bioactivity observed in the heat-treated $TiZrCrNb_{0.25}Ta_{0.05}$ sample. Overall, the findings suggest that the $TiZrCrNb_{0.25}Ta_{0.05}$ alloy has the potential to serve as an alternative biomaterial to the TNTZ alloy, with its bioactivity properties being further enhanced through heat treatment. Further studies are recommended to optimize its bioactivity and evaluate its in-vivo performance for biomedical applications.

Key words: Medium-entropy alloys, TNTZ waste recycling, TiZrCrNbTa alloy, bioactivity, metal ion release.

TNTZ Atıklarından Üretilen $TiZrCrNb_{0.3}Ta_{0.07}$ Orta Entropili Alaşımın Biyoaktivite Özelliklerinin Araştırılması

Öz: Yüksek entropili alaşımlar ve orta entropili alaşımlar, üstün fiziksel ve kimyasal özellikleri sayesinde geleneksel alaşımlara kıyasla çeşitli alanlarda alternatif malzemeler olarak önemli bir ilgi görmektedir. Bu yenilikçi malzeme sınıfının en umut verici uygulama alanlarından biri biyomalzemelerdir. Bu çalışmada, toksik olmayan elementler (Ti, Zr, Cr, Nb ve Ta) kullanılarak, TNTZ alaşımı atığından ark ergitme yöntemiyle başarıyla sentezlenen bir biyo-orta entropili alaşım, $TiZrCrNb_{0.25}Ta_{0.05}$, elde edilmiştir. Üretilen biyo-orta entropili alaşımın yapısal ve kimyasal özellikleri; taramalı elektron mikroskobu, enerji saçınımlı X-ışını spektroskopisi ve X-ışını difraksiyonu teknikleriyle kapsamlı bir şekilde karakterize edilmiştir. Ayrıca, alaşımın in-vitro degradasyon davranışı, iyon salınımı ve biyouyumluluğu değerlendirilmiş ve bu özellikler ısıl işlemin etkisi dikkate alınarak konvansiyonel TNTZ alaşımıyla karşılaştırılmıştır. Elde edilen sonuçlar, ısıl işlemin $TiZrCrNb_{0.25}Ta_{0.05}$ alaşımının mikroyapısında belirgin bir değişikliğe yol açmadığını, ancak yüzeyde Cr_2Zr ve Cr_2Ta gibi intermetalik fazların oluşumuna neden olduğunu göstermiştir. Degradasyon testleri, dört haftalık daldırma süreci sonunda tüm numune gruplarında beklenen kütle kaybının aksine, yüzeydeki çökelmelere bağlı olarak net kütle artışı gözlemlendiğini ortaya koymuştur. İyon salınım analizlerinde, $TiZrCrNb_{0.25}Ta_{0.05}$ ve TNTZ alaşımlarının benzer davranışlar sergilediği ve iyon salınım seviyelerinin ppb aralığında olduğu tespit edilmiş; özellikle salınan titanyum iyonlarının toksik olmayan düzeylerde olduğu doğrulanmıştır. Biyouyumluluk testlerinde, tüm numunelerin yüzeylerinde düşük seviyede Ca-P-O birikimi gözlemlenmiş; en yüksek biyouyumluluk ise ısıl işlem uygulanmış $TiZrCrNb_{0.25}Ta_{0.05}$ numunesinde saptanmıştır. Genel olarak, elde edilen bulgular $TiZrCrNb_{0.25}Ta_{0.05}$ alaşımının TNTZ alaşımına alternatif bir biyomalzeme olarak kullanılabileceğini ve ısıl işlemle biyouyumluluğunun daha da artırılabileceğini göstermektedir. Biyolojik uygulamalarda in-vivo performansının değerlendirilmesi ve biyouyumluluğunun optimize edilmesi için ileri düzey çalışmalar önerilmektedir.

Anahtar kelimeler: Orta entropili alaşımlar, TNTZ atık geri dönüşümü, TiZrCrNbTa alaşımı, biyoaktivite, metal iyon salınımı.

[*] Sorumlu yazar: nhlyayla@gmail.com. Yazarların ORCID Numarası: [1] 0000-0001-7170-4572, [2] 0000-0003-4334-7314, [3] 0000-0001-5005-8516, [4] 0009-0006-2316-136X

1. Introduction

In response to increasing demands for energy efficiency and sustainability, the continuous development of high-performance materials has become imperative. Traditional alloys typically exhibit a structure where the primary element constitutes a significant atomic fraction, while smaller quantities of other alloying elements are added to enhance specific properties. Within this context, an alloy family based on a principal element is formulated, with various alloying elements incorporated to optimize desired performance characteristics [1, 2]. Moreover, due to the limited number of elements available in the periodic table, the range of alloy families that can be developed is inherently constrained. To overcome this limitation and transcend conventional boundaries, a novel alloy concept known as compositionally complex alloys — including high-entropy alloys (HEAs) and medium-entropy alloys (MEAs) — has been introduced [3-5]. This approach is based on combining multiple principal elements, typically in equiatomic ratios and relatively high concentrations. By doing so, the limitations of conventional alloys have been overcome, enabling the design of novel materials with versatile properties [6].

MEAs, which typically contain three to four principal elements, represent a subclass of compositionally complex alloys where the configurational entropy is lower than in HEAs but still significant enough to promote the formation of solid solution phases. While HEAs are defined as alloys that consist of at least five principal metallic elements, each with an atomic percentage ranging between 5% and 35% [7-10], MEAs contain fewer elements and exhibit lower mixing entropy, yet they often demonstrate similar or even superior mechanical and corrosion resistance properties, especially when optimized for biomedical applications [11-13]. According to Yeh and colleagues, HEAs are defined as alloys where the configurational mixing entropy (ΔS_{mix}) dominates the solidification thermodynamics, thereby favoring the formation of random solid solution phases over intermetallic compounds. In their initial studies, they proposed the criterion of $\Delta S_{mix} \geq \ln(5)R$ for HEA castings. This criterion implies the mixing of at least five elements in equiatomic composition [14-16]. For MEAs, the configurational entropy lies in the range of $\ln(3)R \leq \Delta S_{mix} < \ln(5)R$, corresponding typically to alloys containing three or four principal elements in near-equiatomic or non-equiatomic ratios. In the case of MEAs, the ΔS_{mix} value falls below this threshold but remains sufficient to influence phase stability and mechanical behavior [17-20]. The selection of five elements as the lower limit is considered a critical factor to ensure that the mixing entropy is sufficiently high to balance the mixing enthalpy, thereby promoting the formation of solid solution phases [21].

MEAs, like HEAs, exhibit remarkable properties such as high strength, enhanced wear resistance, and excellent corrosion behavior. These properties stem from the interplay of thermodynamic and structural effects similar to those in HEAs. Among these, four fundamental effects have been identified [4, 22, 23]. (i) The high-entropy effect from a thermodynamic perspective; (ii) the sluggish diffusion effect from a kinetic perspective; (iii) the severe lattice distortion effect from a structural standpoint; and (iv) the overall "cocktail effect" arising from the unique interplay of composition, structure, and microstructure [24-26]. Despite the compositional complexity, many MEAs also exhibit simple structures such as face-centered cubic (FCC), body-centered cubic (BCC), or hexagonal close-packed (HCP) phases, rather than forming complex intermetallic compounds. This is attributed to the balance of mixing entropy and enthalpy, which in MEAs is carefully tuned through element selection. The synergistic combination of the four effects, although moderated compared to HEAs, still endows MEAs with outstanding mechanical and chemical properties [27-33]. The performance of HEAs is highly dependent on the manufacturing methods and the parameters employed during synthesis. HEAs are produced using both conventional and advanced alloy synthesis techniques, which can be classified into four main categories based on the state of the elements during the synthesis process: (i) liquid-state synthesis, (ii) solid-state synthesis, (iii) gas-phase synthesis, and (iv) novel synthesis methods, particularly electrochemical processes. These techniques are employed to optimize the structural and mechanical properties of HEAs [34, 35].

In surgical operations, metallic implants are frequently chosen, particularly in hard tissue applications. However, it is known that metallic implants have problems such as low biocompability, inadequate corrosion resistance, mechanical incompatibility, high density and potential ion release, which can lead to toxicity and allergic tissue reactions [36, 37]. The advantages of titanium alloys over stainless steel and Co-Cr alloys include their low density, high strength, corrosion resistance, and biocompatibility [38]. However, titanium alloys are considered bioinert materials, and extensive research efforts are ongoing to enhance their biocompatibility [39, 40]. Due to their superior properties, MEAs and HEAs have the potential to serve as alternatives to conventional alloys in metallic biomaterials. With their high corrosion resistance and biocompatibility, medium-entropy alloys have recently gained attention as a promising subclass within the broader family of Bio-HEAs, often referred to as "Bio-MEAs" when configurational entropy falls within a moderate range. In biomedical applications, these alloys demonstrate promising attributes such as excellent antibacterial properties, exceptional biocompatibility, and outstanding corrosion resistance. These features position Bio-MEAs as an innovative and effective material

class capable of providing advanced solutions in the biomedical field [41-46]. Studies have demonstrated that both HEAs and MEAs have the potential to complement existing materials in biomedical applications [47, 48]. The selection of constituent elements for Bio-HEAs and Bio-MEAs are critically important to ensure biocompatibility and safety. Elements such as Ti, Zr, Hf, Nb, Ta, V, Mo, Mg, Cu, Zn, Co, Cr, W, Ag, Al, and Sn are commonly preferred in these alloys, as they exhibit no toxic effects in implantation sites and pose no risk to tissue cells. For instance, systematic experiments conducted on the Ti-Zr-Hf-Nb-Ta alloy have revealed that these components exhibit no toxicity or allergic complications. Similarly, alloys such as TiTaNbZr, TiMoNbZr, TiMoTaNbZr, TiZrHfNbTa, TiZrHfNb, and TiNbHfTaZrMo stand out as promising biomaterial candidates due to their high mechanical strength, wear resistance, and corrosion resistance [49-52]. Several studies have investigated equimolar and non-equimolar compositions of alloys such as TiTaNbZr, TiMoNbZr, TiMoTaNbZr, TiZrHfNbTa, TiZrHfNb, and TiNbHfTaZrMo as potential metallic biomaterials. These alloys have demonstrated exceptional properties, including high yield strength (800–1600 MPa), high plasticity, and superior wear resistance. The TiNbTaZrMo alloy has been reported to exhibit excellent friction and corrosion resistance alongside good biocompatibility. Similarly, the TiZrHfNbTa alloy has shown high biocorrosion resistance and biocompatibility comparable to that of the Ti6Al4V alloy [53-56]. In addition, alloys such as $Ti_{40}Zr_{40}Nb_5Ta_{15}$ [57], $Ti_{40}Zr_{25}Nb_{25}Ta_5Mo_5$ [58], $TiZrHfNbFe_{0.5}$ [59] and $Ti_{0.5}ZrNbTaMo$ [60] have been observed to exhibit higher wear resistance compared to the Ti6Al4V alloy. These properties position these compositionally complex alloys — especially MEAs — as promising candidates for potential biomaterials.

In this study, TiZrCrNbTa MEAs, which represent a medium-entropy alloy system and have not been previously investigated, were produced using arc melting by utilizing waste from the Ti-29Nb-13Ta-4.6Zr (TNTZ) alloy. Following production, the alloy underwent heat treatment, and the structural changes before and after the treatment were characterized in detail. Additionally, the in-vitro degradation, ion release, and bioactivity properties of this novel alloy were compared with those of TNTZ alloys. The potential of TiZrCrNbTa MEAs as alternative biomaterials was discussed, and the results were interpreted within the context of MEA design principles and found to be consistent with data reported in the literature.

2. Materials and Methods

2.1. Materials

The $TiZrCrNb_{0.25}Ta_{0.05}$ alloy was synthesized by adding equimolar amounts of high-purity (99.5%) elemental Ti, Zr, and Cr powders (supplied by Nanografi) into Ti-29Nb-13Ta-4.6Zr (TNTZ) alloy waste, the chemical composition of which is listed in Table 1. The constituent powders were mixed using a high-energy ball mill (Retsch PM100) at a speed of 200 rpm for 1 hour under an argon atmosphere to achieve a homogeneous mixture. No significant contamination from the milling media was detected in the subsequent XRD and EDS analyses. Following the mixing process, the powder mixture was compacted into pellets at room temperature under a pressure of 100 MPa using a hydraulic press. The resulting pellets were then melted five times using an arc melting process under a protective argon atmosphere to produce Bio-MEA alloys. The produced Bio-MEA alloys underwent homogenization heat treatment at 1000°C for 15 hours in an argon atmosphere. The process flow chart is illustrated in Figure 1.

Table 1. Chemical compositions of TNTZ waste and $TiZrCrNb_{0.3}Ta_{0.07}$ alloy.

	Chemical Composition (wt.%)				
	Ti	**Nb**	**Ta**	**Zr**	**Cr**
TNTZ	52.79	29.00	13.00	4.60	0
$TiZrCrNb_{0.3}Ta_{0.07}$	20.67	12.03	5.47	39.38	22.45

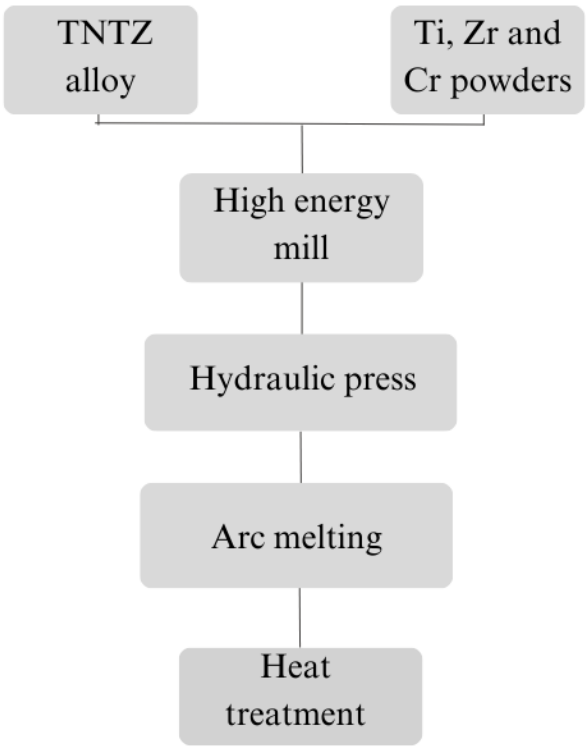

Figure 1. Process flow chart.

2.2. Theorical Calculations

ΔS_{mix}, ΔH_{mix}, VEC, Ω, δ and T_m parameters of the $TiZrCrNb_{0.25}Ta_{0.05}$ alloy were calculated using the High-Entropy Alloys Predicting Software (HEAPS) program [61, 62] and the results are presented in Table 2. The table indicates that the ΔSmix value was calculated as 11.18 J/molK, while the ΔHmix value was determined to be 4.92 kJ/mol. These values fall within the ranges of $-11 \leq \Delta S_{mix} \leq 19.5$ J/molK and $-22 \leq \Delta H_{mix} \leq 7.5$ kJ/mol, meeting the criteria for the formation of a solid solution phase.

The calculated configurational entropy of the alloy, ΔSmix 11.18 J/mol K (≈1.34 R), is slightly less than the generally accepted threshold for high entropy alloys (1.61 R). Therefore, this alloy is categorized as a medium entropy alloy (MEA) according to certain definitions.

Table 2. ΔS_{mix}, ΔH_{mix}, VEC, Ω, δ and T_m values of the $TiZrCrNb_{0.25}Ta_{0.05}$ alloy.

ΔS_{mix} (J/molK)	ΔH_{mix} (kJ/mol)	VEC	Ω	δ (%)	T_m (°C)
11.18	-4.92	4.7	4.89	9.64	1878.85

2.3. Characterization analysis

The microstructure of the reference TNTZ alloy and the synthesized $TiZrCrNb_{0.25}Ta_{0.05}$ alloy, both before and after heat treatment, was comprehensively examined using SEM/EDS (Hitachi SU3500, Oxford AZtech) and XRD (Rigaku Miniflex 600) analyses. Prior to characterization, the surfaces of the samples were polished using a dual-table metallographic grinding and polishing machine (Metkon). XRD analyses were performed with a Cu-Kα tube over a range of 20–90° at a scanning speed of 2°/min.

2.4. In vitro degradation and ion releases

To evaluate the in-vitro bioactivity properties of the $TiZrCrNb_{0.25}Ta_{0.05}$ alloy, a four-week immersion test was conducted in simulated body fluid (SBF). The as-cast and heat-treated structures of the alloy were assessed in

terms of degradation, ion release, and bioactivity properties, and compared with those of the TNTZ alloy. The bioactivity tests were performed in SBF, whose chemical composition is provided in Table 3, at a controlled solution temperature of 37°C for a duration of four weeks. The degradation rates were determined by calculating the weight differences between the samples at the beginning and after the four-week immersion period. Each sample group was tested in triplicate, with standard deviations calculated, and the average values were considered. At the end of the four-week immersion, metal ions released from the samples into the SBF solution were detected using an ICP-MS analyzer (Perkin Elmer NexION 350X). For analysis, 1 ml of the SBF solution was collected, mixed with 1% nitric acid (HNO_3), and diluted appropriately with ultrapure water. Ion release analyses were conducted in triplicate for each sample group, and average results were calculated. To determine the bioactivity on the sample surfaces at the end of the immersion period, comprehensive SEM/EDS and XRD analyses were performed. These analyses aimed to identify Ca-P nucleation on the sample surfaces.

Table 3. Chemical composition of simulated body fluid (SBF) solution [63].

NaCla	8.035 g
$NaHCO_3$	0.355 g
KCl	0.225 g
$K_2HPO_4.3H_2O$	0.231 g
$MgCl_2.6H_2O$	0.311 g
HCl (1 molar)	39.0 mL
$CaCl_2$	0.292 g
Na_2SO_4	0.072 g
$(HOCH_2)_3CNH_2$	6.118 g
HCl (1 Molar)	0-5mL (Appropriate amount to adjust pH to ~7.4)

3. Result and Discussion

Figure 2 presents the XRD analyses of the as-cast and heat-treated structures of the $TiZrCrNb_{0.25}Ta_{0.05}$ MEA and the reference TNTZ alloy prior to degradation. In the XRD pattern of the TNTZ alloy, dominant (β) phase peaks [64] were identified, and these peaks exhibited a homogeneous distribution characteristic of this phase. When comparing the peaks of the alloy's as-cast and heat-treated structures, the presence of characteristic FCC (Face-Centered Cubic) phase peaks at 44° and 75° angles was observed in both samples [65-67]. Additionally, characteristic peaks of the TNTZ alloy were identified at approximately 36°, 54° and 80°. In contrast to the alloy's characteristic peaks, Cr_2Zr peaks were observed at 35°, 41°, 43°, 63°, 67°, 74°, 85° and 89°, while Cr_2Ta peaks were detected at 21° and 30°. Notably, after heat treatment, the Cr_2Ta peak at approximately 30° disappeared, whereas the peak at 21° remained present. These results indicate that the Cr element in the TiZrCrNbTa MEA forms intermetallic compounds with the Zr and Ta elements present in the TNTZ alloy. According to the XRD analysis, the lack of significant differences between the as-cast structure and the heat-treated structure suggests that no new intermetallic compounds were formed after heat treatment. The absence of different phases, despite the application of high-temperature and prolonged heat treatment, indicates the stability of intermetallic compounds formed during the arc melting process. This demonstrates that the heat treatment does not affect the existing phases and does not lead to phase transitions or the formation of new phases within the structure.

The observed FCC phase formation in our $TiZrCrNb_{0.25}Ta_{0.05}$alloy is consistent with findings by [68-70], who reported similar FCC structure in TiZrNbTa-based alloys with Cr additions. However, our results show some distinct differences in peak intensities and positions compared to the equiatomic TiZrCrNbTa alloy studied by which exhibited a predominant BCC structure. This difference can be attributed to our non-equiatomic composition with lower Nb and Ta content, which alters the electron concentration and phase stability. The formation of intermetallic compounds (Cr_2Zr and Cr_2Ta) after heat treatment aligns with observations by who documented similar precipitation behavior in Cr-containing refractory MEAs after prolonged thermal exposure. Interestingly, reported that such intermetallic phases, when present in controlled amounts, can enhance both mechanical properties and bioactivity of Ti-based alloys through microstructural refinement and surface energy modification [71, 72].

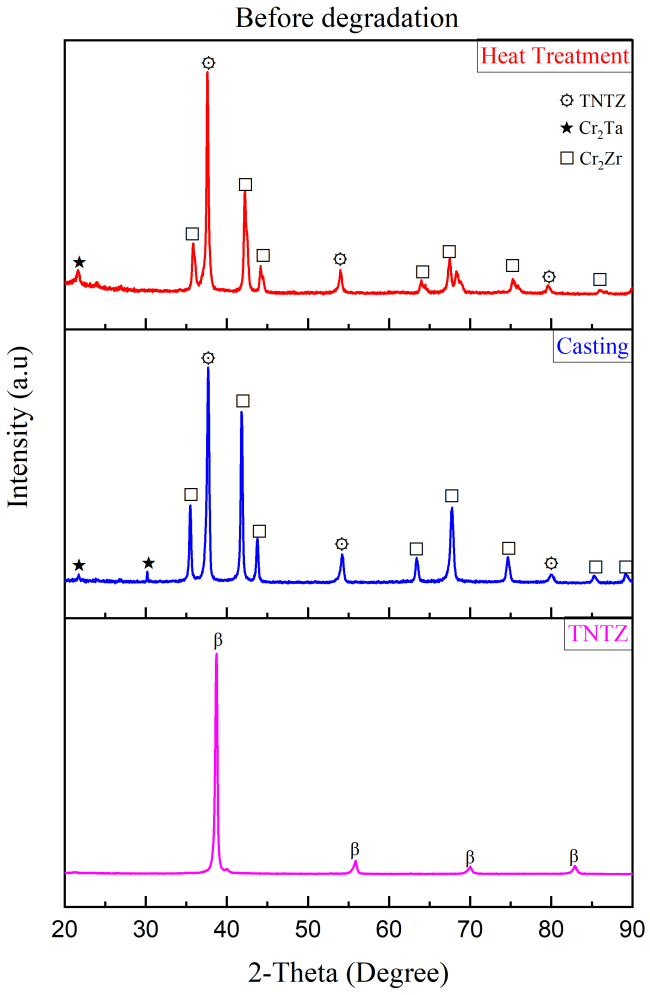

Figure 2. XRD analyses before degradation; TNTZ alloy, casting and heat treatment $TiZrCrNb_{0.25}Ta_{0.05}$ alloy.

Figure 3 presents the EDS elemental mapping images and elemental analysis results of the TNTZ alloy and the $TiZrCrNb_{0.25}Ta_{0.05}$ alloys, both before and after heat treatment, prior to degradation. Figure 3-a shows that the elements constituting the TNTZ alloy are distributed homogeneously throughout the alloy. Similarly, Figure 3-b indicates a homogeneous elemental distribution on the surface of the as-cast $TiZrCrNb_{0.25}Ta_{0.05}$ alloy; however, micro-pores are observed on the surface. Additionally, Zr- and Cr-rich regions were identified in the as-cast structure of the alloy, which are believed to result from rapid cooling or thermal effects during the production process. Similar findings have also been reported by other researchers [73-75]. The Cr_2Zr and Cr_2Ta phases identified in the XRD analysis results support this observation. Figure 3-c shows that the homogeneous elemental distribution was re-established, microstructural irregularities were reduced, yet minor localized accumulations of Cr and Zr elements persisted. According to the EDS elemental analysis results, the TNTZ alloy contains Ti (50.9 wt%), Nb (31.0 wt%), Ta (13.9 wt%), and Zr (4.2 wt%) as its primary constituents. In the as-cast MEA structure, the proportions of Zr (38.5 wt%) and Cr (18.9 wt%) significantly increased, while the Ti and Nb contents decreased. Post-heat treatment EDS spectra were similar to the as-cast structure, but the oxygen content increased slightly from 4.5% to 5.0%. This increase may be attributed to minor surface oxide formation during the heat treatment process.

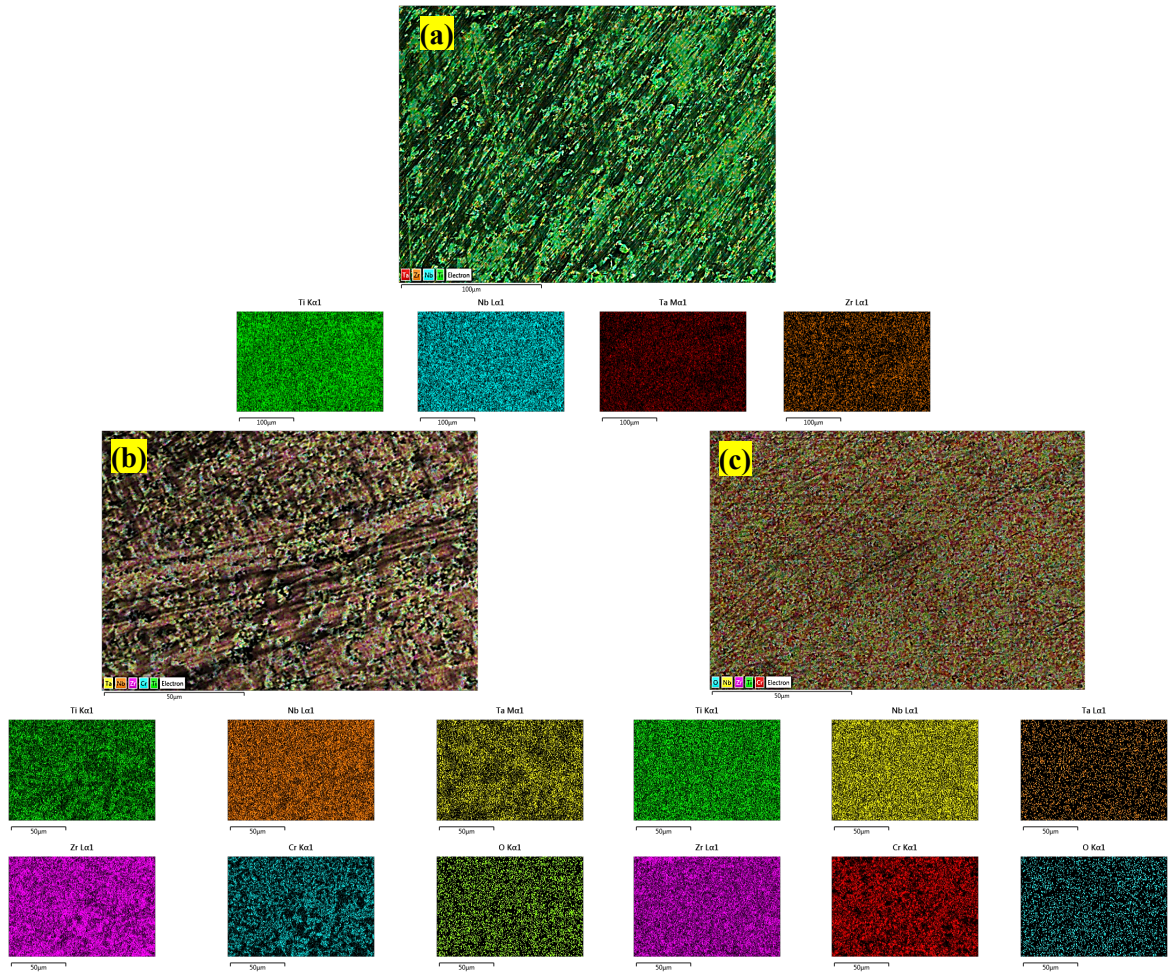

EDS analysis results

Elements	Ti	Nb	Ta	Zr	Cr	Ca	P	O
TNTZ	50.9	31.0	13.9	4.2	-	-	-	-
Casting	21.7	12.0	4.5	38.5	18.9	-	-	4.5
Heat Treatment	21.6	11.5	4.3	38.5	19.1	-	-	5.0

Figure 3. EDS elemental mapping images and elemental analysis results of (a) TNTZ alloy before degradation, (b) before heat treatment and (c) after heat treatment $TiZrCrNb_{0.25}Ta_{0.05}$ alloys.

The XRD analyses presented in Figure 4 illustrate the examination of phase structures in different sample groups. The XRD results of the TNTZ alloy indicate no significant changes in its structure following degradation. According to the analysis, the β-phase remains the dominant crystal structure in the alloy, clearly demonstrating that the degradation process did not significantly affect the crystal structure and that the TNTZ alloy retains its structural stability. Similarly, the as-cast structure of the $TiZrCrNb_{0.25}Ta_{0.05}$ alloy showed no notable differences after degradation, similar to the TNTZ alloy. However, minor shifts in peaks were observed in the XRD analyses, with a notable increase in the intensity of the Cr2Ta peak around 32°. Interestingly, this peak is located in close proximity to characteristic hydroxyapatite peaks typically observed in XRD analyses at 31.7°, 32.9°, and 34.1° [76-78]. This similarity suggests that the phases and precipitates formed on the alloy surface during degradation may exhibit a structure analogous to hydroxyapatite. Furthermore, the increase in peak intensity is thought to result from Ca-P nucleation on the sample surface during the degradation process. The XRD analyses of the heat-treated alloy post-degradation showed results similar to those obtained before degradation, consistent with other groups. However, the emergence of a peak around 32° after degradation supports the presence of Ca-P nucleation on the surface. Nevertheless, XRD analyses alone are insufficient for a comprehensive evaluation of the bioactivity on

the sample surfaces. To thoroughly assess bioactivity, the XRD results must be corroborated with EDS analyses. This combination enables a more detailed investigation of the chemical changes occurring on the surface.

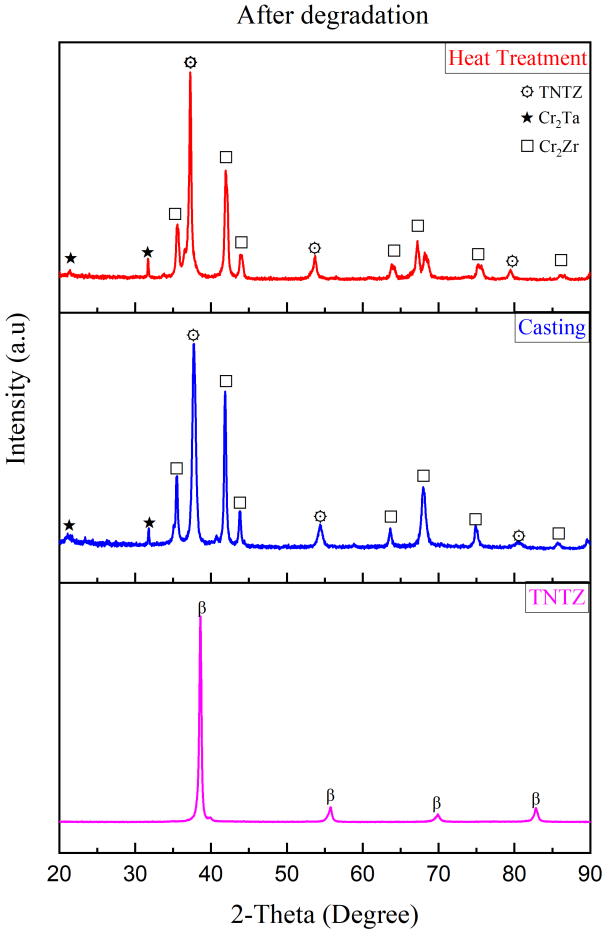

Figure 4. XRD analyses after degradation; TNTZ alloy, casting and heat treatment $TiZrCrNb_{0.25}Ta_{0.05}$ alloy.

Figure 5 presents the EDS elemental mapping images and elemental analysis results of the sample groups after degradation. In Figure 5-a, the TNTZ alloy exhibits a significant increase in surface irregularities and roughness post-degradation. Notably, the linear structures on the surface appear disrupted, and bioactive precipitates are observed on the material's surface. In Figure 5-b, the as-cast $TiZrCrNb_{0.25}Ta_{0.05}$ alloy also shows pronounced surface changes after degradation. Specifically, an increase in micro-pores and a more complex, roughened surface structure are evident. These observations suggest the formation of bioactive phases, such as apatite or salt precipitates, on the material's surface during degradation. Additionally, noticeable surface cracks and increased irregularities are observed, which may indicate an increase in Ca-P nucleation on the material's surface due to chemical interactions. Figure 5-c highlights more prominent morphological changes on the material surface. Bioactive precipitates and irregularities, including Ca-P nucleation, are clearly observed. These irregularities, formed after degradation, indicate that the material encounters Ca-P accumulation in the biological environment, leading to enhanced bioactivity. While microstructural homogeneity decreases, irregular surface structures become apparent. Moreover, the size and distribution of the precipitates suggest that the material's surface becomes more biologically active as a biomaterial. The EDS elemental analysis results post-degradation reveal a significant decrease in major elements such as Ti (48.3 wt%), Nb (25.2 wt%), and Ta (11.7 wt%). This reduction implies that chemical reactions and surface degradation have led to mass loss in the primary components of the material. In particular, the decrease in Nb and Ta content suggests that these elements are more prone to dissolution in the SBF medium or may be displaced during apatite formation on the surface. Compared to pre-degradation conditions, the presence of oxygen (13.7 wt%), calcium (0.1 wt%), and phosphorus (1.0 wt%) indicates the formation of Ca-P nucleation and bioactive phases such as apatite on the surface. The increase in

oxygen content further supports intensified oxidation processes on the surface, aligning with the observed enhancement in the material's bioactivity. These findings highlight the potential of the alloy as an active biomaterial in biological environments.

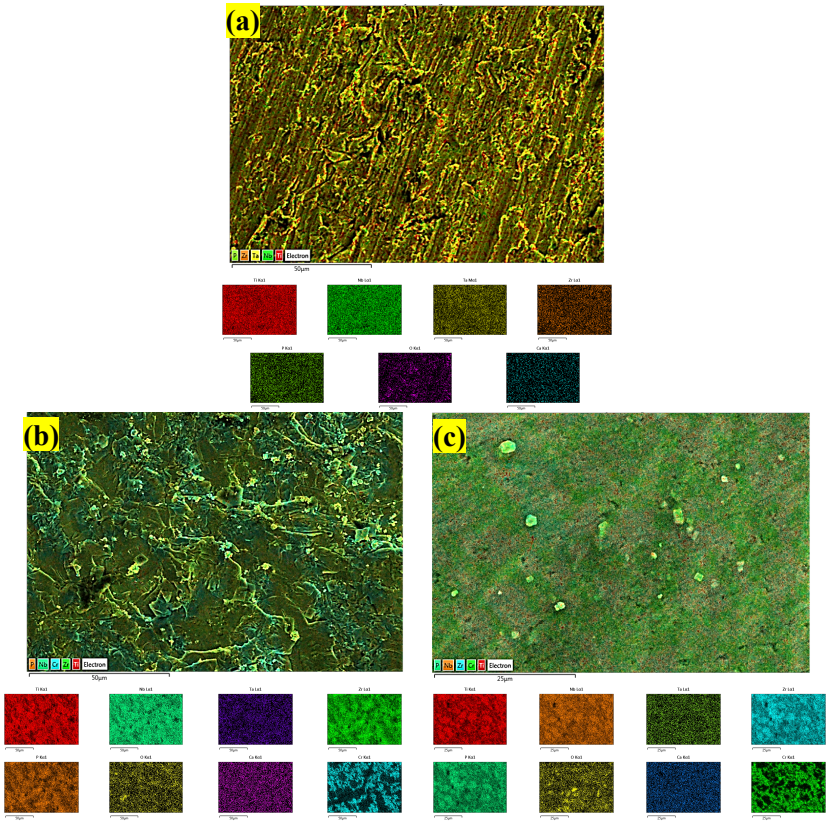

Elements	Ti	Nb	Ta	Zr	Cr	Ca	P	O
TNTZ	48.3	25.2	11.7	-	-	0.1	1.0	13.7
Casting	21.2	14.2	7.1	28.3	26.7	0.2	0.2	2.0
Heat Treatment	16.7	9.8	5.4	29.7	21.5	0.1	0.5	15.4

Figure 5. EDS elemental mapping images and elemental analysis results of (a) TNTZ alloy after degradation, (b) before heat treatment and (c) after heat treatment $TiZrCrNb_{0.25}Ta_{0.05}$ alloys.

Table 4 presents the degradation results of the alloy samples after a four-week immersion period in SBF. Degradation in biomaterials refers to the mass loss that occurs due to chemical or biological breakdown when the material interacts with body fluids. However, contrary to expectations, the results indicate a mass increase rather than a loss across all sample groups. This phenomenon suggests that surface precipitations during immersion in SBF were more dominant than mass loss due to degradation. For the TNTZ alloy, the degradation percentages ranged between -2.11% and -2.28%, with an average value of -1.74%. In the as-cast $TiZrCrNb_{0.25}Ta_{0.05}$ alloy, the degradation percentages ranged from -1.03% to -2.13%, with an average of -1.66%. Meanwhile, the heat-treated $TiZrCrNb_{0.25}Ta_{0.05}$ alloy exhibited degradation percentages ranging from -1.24% to -1.86%, with an average of -1.58%. The observed negative degradation percentages indicate that the precipitation processes occurring on the sample surfaces during immersion led to mass accumulation. This is consistent with other studies in the literature, where surface deposition of bioactive phases, such as calcium phosphate (Ca-P), was found to significantly contribute to mass gain in similar SBF immersion experiments. The formation of such bioactive phases highlights the potential of these alloys for use as biomaterials, as the precipitates likely represent apatite-like phases associated with enhanced bioactivity. The slightly lower degradation rates in the heat-treated $TiZrCrNb_{0.25}Ta_{0.05}$ alloy compared to its as-cast counterpart could be attributed to the increased surface homogeneity and structural stability provided by heat treatment. These findings align with prior research demonstrating that heat-treated alloys

often exhibit reduced susceptibility to degradation due to improved structural integrity and reduced microstructural irregularities [79-82]. In conclusion, the mass increase observed in all sample groups reflects the dominant role of surface precipitation over degradation. This suggests that the $TiZrCrNb_{0.25}Ta_{0.05}$ alloy, both in its as-cast and heat-treated forms, possesses strong potential as a bioactive material, capable of promoting the formation of bioactive layers in simulated physiological conditions. Future studies should focus on correlating these findings with in-vivo performance to validate the material's suitability for biomedical applications.

Table 4. Degradation amounts of alloys after four weeks of waiting.

Alloy	Measurement	Before Degradation (g)	After Degradation (g)	Difference (g)	% Degradation	Average	Standard Deviation
TNTZ	1	11.7736	12.0216	-0.248	-2.11	-1.74	0.79
	2	11.9305	12.0282	-0.0977	-0.82		
	3	12.4975	12.7824	-0.2849	-2.28		
$TiZrCrNb_{0.25}Ta_{0.05}$ casting structure	1	12.0484	12.2684	-0.22	-1.83	-1.66	0.57
	2	12.2828	12.4094	-0.1266	-1.03		
	3	11.5922	11.8388	-0.2466	-2.13		
$TiZrCrNb_{0.25}Ta_{0.05}$ heat treated	1	10.8417	10.9762	-0.1345	-1.24	-1.58	0.31
	2	12.4926	12.7244	-0.2318	-1.86		
	3	12.6705	12.8777	-0.2072	-1.64		

Figure 6 illustrates the ion release amounts (ppb/mm²) of the samples immersed in SBF for four weeks. Regarding Ti release, similar amounts were observed for the TNTZ alloy, as-cast, and heat-treated $TiZrCrNb_{0.25}Ta_{0.05}$ alloys. However, a slight reduction in Ti release was noted in the heat-treated samples, likely due to improved surface stability. Nb release was negligible across all samples, with no significant increase or decrease observed after heat treatment, indicating that Nb remains chemically stable under these conditions. Ta release was relatively high in the TNTZ alloy but substantially decreased in both as-cast and heat-treated $TiZrCrNb_{0.25}Ta_{0.05}$ alloys, suggesting that Ta becomes less soluble when incorporated into the high-entropy alloy system. Zr release exhibited an increase in the as-cast and heat-treated samples compared to the TNTZ alloy, with the heat-treated samples showing a pronounced elevation. This suggests that heat treatment enhances the dissolution of Zr, potentially due to microstructural changes such as grain refinement or phase redistribution. Cr release was observed exclusively in the high-entropy alloys, with a significant increase following heat treatment. This behavior indicates that Cr dissolution is strongly influenced by the surface properties altered during heat treatment. Overall, the ion release data suggest that heat treatment impacts the surface characteristics and solubility of certain elements, particularly Zr and Cr. These findings are consistent with other studies in the literature, which report that heat treatment can modify the surface chemistry and microstructure of high-entropy alloys, thereby affecting their ion release behavior in simulated physiological environments. Such alterations could have implications for the bioactivity and biocompatibility of the materials, as higher ion release may correlate with enhanced surface reactivity and Ca-P nucleation in SBF conditions [83-85].

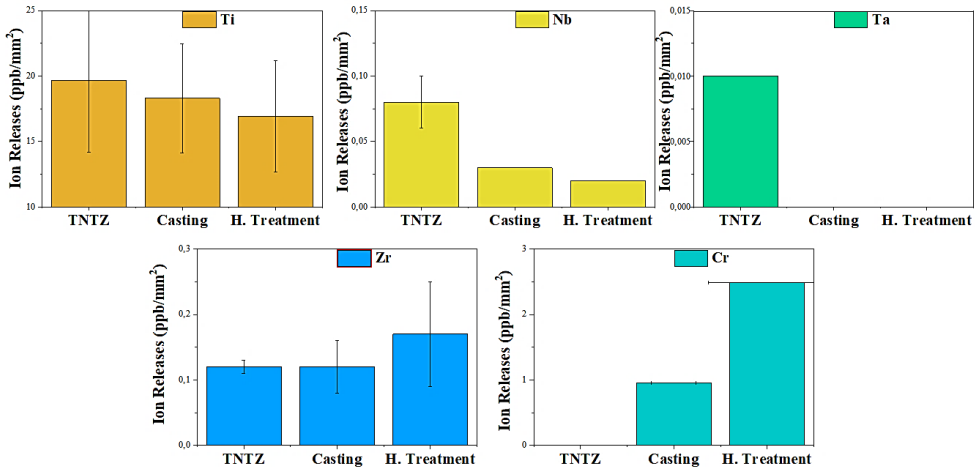

Figure 6. Ion release amounts of samples kept in SBF environment for four weeks (ppb/mm²).

4. Conclusion

In this study, the $TiZrCrNb_{0.25}Ta_{0.05}$ medium-entropy alloy (MEA) was successfully synthesized using Ti-29Nb-13Ta-4.6Zr (TNTZ) waste through arc melting, followed by homogenization heat treatment. Structural characterization, degradation behavior, ion release, and bioactivity analyses were conducted, yielding the following key findings:

- Structural Analysis: No significant structural differences were observed between the as-cast and heat-treated samples, indicating stability in the microstructure.
- Intermetallic Compound Formation: The addition of Cr to the TNTZ waste resulted in the formation of certain intermetallic compounds within the alloy matrix. XRD analysis confirmed the formation of a dominant FCC phase in the as-cast alloy, with the development of Cr_2Zr and Cr_2Ta intermetallic compounds upon heat treatment.
- Degradation Analysis: After a four-week immersion in SBF, all sample groups exhibited mass gain rather than mass loss. This indicates that surface precipitation processes, particularly the formation of bioactive layers, outweighed the effects of material degradation.
- Ion Release: The ion release behavior of the synthesized MEA was comparable to that of the TNTZ alloy. Ti ions were detected in all samples, with release levels remaining in the ppb range, suggesting excellent corrosion resistance.
- Bioactivity Analysis: The presence of Ca-P-O phases was detected in low amounts on all sample surfaces, with the highest bioactivity observed in the heat-treated $TiZrCrNb_{0.25}Ta_{0.05}$ alloy.
- General Findings: The degradation, ion release, and bioactivity results demonstrate that the $TiZrCrNb_{0.25}Ta_{0.05}$ alloy exhibits properties similar to those of the TNTZ alloy. Notably, the heat-treated alloy exhibited superior bioactivity, suggesting its potential as an alternative biomaterial to TNTZ.

In conclusion, the $TiZrCrNb_{0.25}Ta_{0.05}$ MEA synthesized in this study has shown promise as a potential biomaterial, particularly when subjected to heat treatment. These structural features, combined with the observed low ion release and enhanced bioactivity after heat treatment, support the alloy's potential as an alternative biomaterial to TNTZ. However, further research is necessary to enhance its bioactivity properties and to evaluate its in-vivo performance for practical biomedical applications.

References

[1] Senkov O, Miller J, Miracle D, Woodward C. Accelerated exploration of multi-principal element alloys with solid solution phases. Nat Commun 2015; 6(1):6529.
[2] Lu Z, Wang H, Chen M, Baker I, Yeh J, Liu C, et al. An assessment on the future development of high-entropy alloys: Summary from a recent workshop. Intermetallics. 2015; 66:67-76.
[3] Tsai M-H, Yeh J-W. High-entropy alloys: a critical review. Mater Res Lett 2014; 2(3):107-23.
[4] Yeh J-W. Alloy design strategies and future trends in high-entropy alloys. Jom. 2013; 65:1759-71.

[5] Wu X. Chemical short-range orders in high-/medium-entropy alloys. J Mater Sci Technol 2023; 147:189-96.
[6] George EP, Ritchie RO. High-entropy materials. MRS Bull 2022; 47(2):145-50.
[7] Miracle DB, Miller JD, Senkov ON, Woodward C, Uchic MD, Tiley J. Exploration and development of high entropy alloys for structural applications. Entropy. 2014; 16(1):494-525.
[8] Zhang W, Liaw PK, Zhang Y. Science and technology in high-entropy alloys. Sci China Mater 2018; 61(1):2-22.
[9] Gao MC, Yeh J-W, Liaw PK, Zhang Y. High-entropy alloys: fundamentals and applications: Springer; 2016.
[10] Zhang Y, Yang X, Liaw P. Alloy design and properties optimization of high-entropy alloys. Jom. 2012; 64:830-8.
[11] Wong K-K, Hsu H-C, Wu S-C, Ho W-F. A review: Design from beta titanium alloys to medium-entropy alloys for biomedical applications. Materials 2023; 16(21):7046.
[12] Xu X, Li Z, Lai W, Wang B, Xu Q, Zhang Z, et al. Improved wear and corrosion resistance of biomedical TiZrNbTaMo medium-entropy alloy by thermal oxidation treatment. Tribol Int 2023; 189:108897.
[13] Zhu D, Li X, Chai S, Chee T-S, Kim C, Li L, et al. Evaluation of wear, corrosion, and biocompatibility of a novel biomedical TiZr-based medium entropy alloy. J Mech Behav Biomed Mater 2025:106951.
[14] Miracle DB, Senkov ON. A critical review of high entropy alloys and related concepts. Acta Mater 2017; 122:448-511.
[15] Ye Y, Wang Q, Lu J, Liu C, Yang Y. High-entropy alloy: challenges and prospects. Mater Today 2016; 19(6):349-62.
[16] Zhang LS, Ma GL, Fu LC, Tian JY. Recent progress in high-entropy alloys. Adv Mater Res. 2013; 631:227-32.
[17] Zhou H, Mao J, Jiang H, Zhang H, Wei W, Qin S, et al. Effect of rare-earth element Y addition on microstructure and mechanical properties of CrFeNi2 medium entropy alloy. Intermetallics. 2023; 163:108079.
[18] Lin S, Lai W, Vogel F, Tong X, You D, Li W, et al. Mechanical and corrosion properties of biomedical (TiZr) 90-xNbxTa5Mo5 medium entropy alloys. Int J Refract Met Hard Mater 2023; 116:106361.
[19] Odetola PI, Babalola BJ, Afolabi AE, Anamu US, Olorundaisi E, Umba MC, et al. Exploring high entropy alloys: A review on thermodynamic design and computational modeling strategies for advanced materials applications. Heliyon. 2024.
[20] Bu QZ, Zhang JX, Zhang HR, Li R, Zhang T, Liu L, et al. Separating the Role of Mixing-Entropy on the Dynamics of Glass-Forming Liquids. Adv Sci 2025:2502568.
[21] Jien-Wei Y. Recent progress in high entropy alloys. Ann. Chim. Sci. Mat. 2006; 31(6):633-48.
[22] Senkov O, Miller J, Miracle D, Woodward C. Accelerated exploration of multi-principal element alloys for structural applications. Calphad. 2015; 50:32-48.
[23] MacDonald B, Fu Z, Zheng B, Chen W, Lin Y, Chen F, et al. Recent progress in high entropy alloy research. Jom 2017; 69:2024-31.
[24] Zhang Y, Zuo TT, Tang Z, Gao MC, Dahmen KA, Liaw PK, et al. Microstructures and properties of high-entropy alloys. Prog Mater Sci 2014; 61:1-93.
[25] Hsu W-L, Tsai C-W, Yeh A-C, Yeh J-W. Clarifying the four core effects of high-entropy materials. Nat Rev Chem 2024:1-15.
[26] Murty BS, Yeh J-W, Ranganathan S, Bhattacharjee PP. High-entropy alloys: Elsevier; 2019.
[27] Li W, Xie D, Li D, Zhang Y, Gao Y, Liaw PK. Mechanical behavior of high-entropy alloys. Prog Mater Sci 2021; 118:100777.
[28] Yeh JW, Chen YL, Lin SJ, Chen SK, editors. High-entropy alloys–a new era of exploitation. Mater Sci Forum; 2007: Trans Tech Publ.
[29] Yang Y-C, Liu C, Lin C-Y, Xia Z. Core effect of local atomic configuration and design principles in AlxCoCrFeNi high-entropy alloys. Scr Mater 2020; 178:181-6.
[30] X. Chang MZ, K. Liu, L. Fu. Phase engineering of high-entropy alloys. Adv. Mater. 2020; 32(14):1907226.
[31] Kozak R, Sologubenko A, Steurer W. Single-phase high-entropy alloys–an overview. Z Kristallogr Cryst Mater 2015; 230(1):55-68.
[32] Shuai C, Xie J, Jiang X, Peng S, Wang C. Additively manufactured high entropy alloy with high wear resistance for biomedical implant. Vacuum. 2024; 221:112939.
[33] Xu D, Wang M, Li T, Wei X, Lu Y. A critical review of the mechanical properties of CoCrNi-based medium-entropy alloys. Microstructures. 2022; 2(1):N/A-N/A.
[34] Alshataif YA, Sivasankaran S, Al-Mufadi FA, Alaboodi AS, Ammar HR. Manufacturing methods, microstructural and mechanical properties evolutions of high-entropy alloys: a review. Met. Mater. Int. 2020; 26:1099-133.
[35] Kumari P, Gupta AK, Mishra RK, Ahmad M, Shahi RR. A comprehensive review: recent progress on magnetic high entropy alloys and oxides. J Magn Magn Mater 2022; 554:169142.
[36] Leyens C, Peters M. Titanium and titanium alloys: fundamentals and applications: Wiley Online Library; 2006.
[37] Veiga C, Davim JP, Loureiro A. Properties and applications of titanium alloys: a brief review. Rev Adv Mater Sci 2012; 32(2):133-48.
[38] Zhang LC, Chen LY. A review on biomedical titanium alloys: recent progress and prospect. Adv Eng Mater 2019; 21(4):1801215.
[39] Bandyopadhyay A, Mitra I, Goodman SB, Kumar M, Bose S. Improving biocompatibility for next generation of metallic implants. Prog Mater Sci 2023; 133:101053.
[40] Khan FS, Khalid M, Ali AH, Bazighifan O, Ghanim F. Results Eng.
[41] Ahmady AR, Ekhlasi A, Nouri A, Nazarpak MH, Gong P, Solouk A. High entropy alloy coatings for biomedical applications: A review. Smart Mater Manuf 2023; 1:100009.

[42] Castro D, Jaeger P, Baptista AC, Oliveira JP. An overview of high-entropy alloys as biomaterials. Metals. 2021; 11(4):648.
[43] Shi Z, Fang Q, Liaw PK, Li J. Corrosion-Resistant Biomedical High-Entropy Alloys: A Review Adv Eng Mater 2023; 25(22):2300968.
[44] San S, Adhikari P, Sakidja R, Brechtl J, Liaw PK, Ching W-Y. Porosity modeling in a TiNbTaZrMo high-entropy alloy for biomedical applications. RSC Adv 2023; 13(51):36468-76.
[45] Bololoi AE, Geambazu LE, Antoniac IV, Bololoi RV, Manea CA, Cojocaru VD, et al. Solid-State Processing of CoCrMoNbTi High-Entropy Alloy for Biomedical Applications. Materials. 2023; 16(19):6520.
[46] Say Y. Synthesis and characterization of TiNbZrMo medium-entropy bio-composites: Microstructure, mechanical properties, and in vitro degradation. J Biomed Mater Res B Appl Biomater 2024; 112(6):e35415.
[47] de Oliveira TG, Fagundes DV, Capellato P, Sachs D, da Silva AAAP. A review of biomaterials based on high-entropy alloys. Metals 2022; 12(11):1940.
[48] Gokcekaya O, Ishimoto T, Nishikawa Y, Kim YS, Matsugaki A, Ozasa R, et al. Novel single crystalline-like non-equiatomic TiZrHfNbTaMo bio-high entropy alloy (BioHEA) developed by laser powder bed fusion. Mater Res Lett 2023; 11(4):274-80.
[49] Feng J, Tang Y, Liu J, Zhang P, Liu C, Wang L. Bio-high entropy alloys: Progress, challenges, and opportunities. Front Bioeng Biotechnol 2022; 10:977282.
[50] Li C, Ma Y, Yang X, Hou M. New TiTaNbZrMo high-entropy alloys for metallic biomaterials. Mater Res Express 2021; 8(10):105403.
[51] Xiang T, Du P, Bao W, Cai Z, Li K, Xie G. Bimodal grain size structure design to optimize the mechanical properties of TiZrNbTa high entropy alloys/Ti composites. Mater Sci Eng A 2022; 849:143488.
[52] Zhu D, Hu S, Fu Y, Zhao N, Liu D. A review of preparation methods, friction and wear, corrosion, and biocompatibility of biomedical high-entropy alloys. J Mater Sci 2024; 59(4):1153-83.
[53] Yang W, Pang S, Liu Y, Wang Q, Liaw PK, Zhang T. Design and properties of novel Ti–Zr–Hf–Nb–Ta high-entropy alloys for biomedical applications. Intermetallics. 2022; 141:107421.
[54] Yang W, Liu Y, Pang S, Liaw PK, Zhang T. Bio-corrosion behavior and in vitro biocompatibility of equimolar TiZrHfNbTa high-entropy alloy. Intermetallics. 2020; 124:106845.
[55] Zhao X, Huang H, Su Y, Qiao L, Yan Y. Exploring high corrosion-resistant refractory high-entropy alloy via a combined experimental and simulation study. npj Mater Degrad 2024; 8(1):77.
[56] Rajabi M, Dehghani K, Shahmir H. Development of a novel Ti35Nb25Zr15Mo15V10 high-entropy alloy for metallic biomaterials. Phys B Condens Matter 2024:416283.
[57] Li Z, Lai W, Tong X, You D, Li W, Wang X. Design of TiZrNbTa multi-principal element alloys with outstanding mechanical properties and wear resistance. Mater Sci Eng A 2022; 845:143203.
[58] Mustafi L, Nguyen VT, Song T, Deng Q, Murdoch BJ, Chen X-B, et al. A strong and ductile biocompatible Ti40Zr25Nb25Ta5Mo5 high entropy alloy. J Mater Res Technol 2024; 30:7885-95.
[59] Wang W, Yang K, Wang Q, Dai P, Fang H, Wu F, et al. Novel Ti-Zr-Hf-Nb-Fe refractory high-entropy alloys for potential biomedical applications. J Alloys Compd 2022; 906:164383.
[60] Hu S, Li T, Su Z, Meng S, Jia Z, Liu D. A novel TiZrNb medium entropy alloy (MEA) with appropriate elastic modulus for biocompatible materials. Mater Sci Eng B 2021; 270:115226.
[61] Martin P, Madrid-Cortes CE, Cáceres C, Araya N, Aguilar C, Cabrera JM. HEAPS: A user-friendly tool for the design and exploration of high-entropy alloys based on semi-empirical parameters. Comput Phys Commun 2022; 278:108398.
[62] Blázquez JS, Manchón-Gordón AF, Vidal-Crespo A, Caballero-Flores R, Ipus JJ, Conde CF. Revisiting Stability Criteria in Ball-Milled High-Entropy Alloys: Do Hume–Rothery and Thermodynamic Rules Equally Apply? Adv Eng Mater 2024:2401148.
[63] Kokubo T, Takadama H. How useful is SBF in predicting in vivo bone bioactivity? Biomaterials. 2006; 27(15):2907-15.
[64] Liu G-L, Wang W, Ma W, Guo S, Shen B-G, Liu H-X. A novel Nb–TiNb nanocomposite with single-phase BCC structure for bio-implant applications. Rare Met 2024:1-8.
[65] Guo Y, Yang F, Lu B, Qiu H, Zhu J, Wang D, et al. Competitive relationship between the FCC+ BCC dual phases in the wear mechanism of laser cladding FeCoCrNiAl0. 5Ti0. 5 HEAs coating. Surf Coat Technol 2024; 493:131315.
[66] Panda J, Arya P, Guruvidyathri K, Ravikirana, Murty B. Studies on kinetics of BCC to FCC phase transformation in AlCoCrFeNi equiatomic high entropy alloy. Metall Mater Trans A 2021; 52:1679-88.
[67] Torrento JE, Sousa TdSPd, Cristino da Cruz N, Santos de Almeida G, Zambuzzi WF, Grandini CR, et al. Development of non-equiatomic Bio-HEAs based on TiZrNbTa-(Mo and Mn). APL Mater 2022; 10(8).
[68] Lai C-Y, Chen Y-I. Structural, mechanical, and anticorrosive properties of (TiZrNbTa) Nx films. J Mater Res Technol 2023; 26:8327-36.
[69] Lushnikov S, Filippova T, Mitrokhin S. Hydride Phases Based on TiZrNbTa (Mo1–xVx)(0< x< 1) High-Entropy Alloys. Inorg Mater 2024; 60(11):1337-43.
[70] Zhang S, Chen L, Stepanov A, Lapteva O, Kholodnaya G, Yu X, et al., editors. Irradiation effect of intense pulsed ion beam on (TiZrNbTaCr) C. Proc. 8th Int. Congr. Energy Fluxes Radiat. Eff. 2022.
[71] Su W, Chen L, Huo S, Zhang W, Wang Y, Zhou Y. Fracture mode transition from intergranular to transgranular in (TiZrNbTaCr) C: the grain boundary purification effect of Cr carbide. J Eur Ceram Soc 2024; 44(4):1881-9.
[72] Su W, Chen L, Zhang W, Huo S, Wang Y, Zhou Y. Insights into grain boundary segregation and solubility limit of Cr in (TiZrNbTaCr) C. J Mater Sci Technol 2023; 139:1-9.

[73] Yi J, Yang L, Wang L, Xu M. Lightweight, Refractory High-Entropy Alloy, CrNbTa 0.25 TiZr, with High Yield Strength. Met Mater Int 2022:1-8.
[74] Inoue A. Stabilization of metallic supercooled liquid and bulk amorphous alloys. Acta Mater. 2000; 48(1):279-306.
[75] Senkov O, Woodward C. Microstructure and properties of a refractory NbCrMo0. 5Ta0. 5TiZr alloy. Mater Sci Eng A 2011; 529:311-20.
[76] Rabiei M, Palevicius A, Monshi A, Nasiri S, Vilkauskas A, Janusas G. Comparing methods for calculating nano crystal size of natural hydroxyapatite using X-ray diffraction. Nanomaterials. 2020; 10(9):1627.
[77] Figueroa-Rosales EX, Martínez-Juárez J, García-Díaz E, Hernández-Cruz D, Sabinas-Hernández SA, Robles-Águila MJ. Photoluminescent properties of hydroxyapatite and hydroxyapatite/multi-walled carbon nanotube composites. Crystals. 2021; 11(7):832.
[78] Serhiienko A, Dontsova T, Yanushevska O, Lapinskyi A, Krymets G. Synthesis and characterization of hydroxyapatite and composite based on it with collagen/alginate. Chem Pap 2021:1-8.
[79] Par M, Gubler A, Attin T, Tarle Z, Tarle A, Tauböck TT. Ion release and hydroxyapatite precipitation of resin composites functionalized with two types of bioactive glass. J Dent 2022; 118:103950.
[80] Temiz A, Alshemary AZ, Akar N, Yaşar M. Rapid casting of biodegradable porous magnesium scaffolds and electrophoretic deposition of 45S5 bioactive glass nanoparticles coatings on porous scaffolds: characterization and in vitro bioactivity analysis. Int J Met Cast 2023; 17(3):1871-82.
[81] Mahato A, De M, Bhattacharjee P, Kumar V, Mukherjee P, Singh G, et al. Role of calcium phosphate and bioactive glass coating on in vivo bone healing of new Mg–Zn–Ca implant. J Mater Sci Mater Med 2021; 32(5):55.
[82] Sfikas AK, Lekatou AG, Emmanouilidou S, Tsirka K. Corrosion Behavior of As-Cast and Heat-Treated Al–Co Alloys in 3.5 wt% NaCl. Mater 2024; 17(3):655.
[83] Guo W, Li J, Qi M, Xu Y, Ezatpour HR. Effects of heat treatment on the microstructure, mechanical properties and corrosion resistance of AlCoCrFeNiTi0. 5 high-entropy alloy. J Alloys Compd 2021; 884:161026.
[84] Huaizhi Q, Minglong G, Dongdong Z, Wenda S, Fengfang L, Jing B, et al. Effect of heat treatment time on the microstructure and properties of FeCoNiCuTi high-entropy alloy. J Mater Res Technol 2023; 24:4510-6.
[85] Liang H, Hou J, Jiang L, Qi Z, Zhang M, Cao Z. The Effect of Heat Treatment on the Microstructure and Mechanical Properties of Al0. 6CoFeNi2V0. 5 High Entropy Alloy Coatings 2024; 14(6):658.